Heat transfer model analysis of fractional Jeffery-type hybrid nanofluid dripping through a poured microchannel

Ali Raza [a,b], Ovidiu V. Stadoleanu [c], Ahmed M. Abed [d,e], Ali Hasan Ali [f,g,h,i,*],
Mohammed Sallah [j]

[a] Department of Mathematics, Minhaj University Lahore, Pakistan
[b] Department of Mathematics, University of Engineering and technology Lahore, Pakistan
[c] Department of Mechanical Engineering and Automotive, Faculty of Mechanical Engineering, "Gheorghe Asachi" Technical University of Iasi, Romania
[d] Department of the Industrial Engineering, College of Engineering, Prince Sattam Bin Abdulaziz University, Al Kharj, 16273, Saudi Arabia
[e] Industrial Engineering Department, Zagazig University, Zagazig, 44519, Egypt
[f] Institute of the Mathematics, University of Debrecen, Pf. 400, H-4002, Debrecen, Hungary
[g] Jadara University Research Center, Jadara University, Irbid 21110, Jordan
[h] Technical Engineering College, Al-Ayen University, Dhi Qar 64001, Iraq
[i] Department of Business Management, Al-imam University College, Balad, Iraq
[j] Department of Physics, College of Sciences, University of Bisha, P.O. Box 344, Bisha 61922, Saudi Arabia

ARTICLE INFO

ABSTRACT

This study investigates the impact of coupled heat and mass transfer on the peristaltic migration of a magnetohydrodynamic (MHD) stress-strain Jeffery-type hybrid nanofluid flowing through an inclined asymmetric micro-channel with a porous medium. The fundamental two-dimensional momentum and energy transport equations are simplified under the assumptions of long wavelength and low Reynolds number. To solve the momentum and heat transfer problems, two advanced fractional derivative approaches are employed: the fractal integral and the Prabhakar fractional derivative. The pressure difference is determined using numerical integration techniques, such as the Stehfest and Tzou's algorithms. The results are presented through graphs and tables, which illustrate the effects of various parameters on the velocity, heat transfer, and trapping phenomena. As a result, we concluded that, pressure gradients grow with higher Reynolds numbers and channel-inclined angles. The heat transfer rate is observed to decrease as the Darcy number and the orientation of the electromagnetic field increase. When comparing the fractional derivative approaches, the fractal operator exhibits a more significant impact on the momentum profiles compared to the Prabhakar fractional operator. This difference is attributed to the distinct characteristics of the integral kernels associated with each fractional derivative definition. Furthermore, when comparing hybrid nanofluids, water-based ($H_2O + Ag + TiO_2$) hybrid fluids have a somewhat more significant effect than ($C_6H_9NaO_7 + Ag + TiO_2$) hybrid nanofluids.

1. Introduction

For many years, researchers have been working to enhance the thermal characteristics of base fluids. To achieve this, the most effective method, initially introduced by Choi [1], is the incorporation of a variety of nanoparticle dispersions into the base materials. This combination of the base fluid and nanoparticles is referred to as "nanofluids". Nanofluids consist of small-sized particles that exhibit improved thermodynamic processes due to factors such as thermal stability, particle interactions, viscosity, temperature dependence, and material

conductivity. The expanding research on nanofluids has enabled numerous commercial applications in diverse fields, including heat engineering, thermal equipment, manufacturing processes, water and soil-based systems, biomedical technologies (e.g., cancer therapy), petroleum engineering, chemical reactions, and nuclear power plants. Scientists have leveraged the unique thermal transport properties and topologies of nanofluids to make various contributions in this area. By applying a dual nano-phase model in annuli having concentric walls, Turkyilmazoglu [2] reported the thermal findings for nanofluids. Using microbial cells in a three-dimensional movable space, Sohail et al. [3]

carried out the optimized structure for nanoparticle flow. Even though the creation of nanofluids has addressed the bulk of industrial objectives, scientists and researchers have continued to seek a more trustworthy and efficient fluid. To fill this void, a novel type of nanofluid was created by merging two different types of nanoparticles with ordinary fluids. Wole-Osho et al. [4] demonstrated the effect of a nanoparticle's mixture ratio, along with temperature and concentration, affecting the thermal conductivity of hybrid nanofluids. Hybrid nanofluids represent a more advanced classification of nanofluids, and the process of creating them is referred to as hybridization. The hybridization of two or more distinct nanoparticles leads to an improvement in the thermal conductivity of the individual nanoparticles, resulting in a novel composition of nanoparticles known as hybrid nanoparticles. Waini et al. [5] studied the continuous, fully formed mixed conduction flow of a longitudinally vertical surface immersed in a porous liquid incorporating hybrid nanoparticles. Pandya et al. [6] focused on a numerical model designed to improve the energy efficiency of an axially walled elevated tunnel utilizing water-based hybrid nano-liquid. Asadi et al. [7] examined the effect of hybrid nano-liquid on system productivity. Nadeem et al. [8] researched a base fluid that ends in an exponentially growing curved surface. The study evaluates the effect of incorporating constraints of the hybrid nanoelement. Waeli et al. [9] investigated hybrid solar power solutions using nanofluid-based filters.

The field of fractional calculus has gained significant attention in various research domains due to its ability to effectively capture the memory effects inherent in many physical phenomena. Fractional calculus is employed in many scientific disciplines, including electrochemistry, biophysics and fluid elasticity [10]. First, in 1967, Caputo presented the fractional operator by utilizing the Laplace transformation and power-law forms together with fractional derivatives. This fractional derivative was the first to solve the Riemann–Liouville operator problem. The singular kernel of this operator, however, contains some flaws in the form of fictitious solutions at $t = \mathscr{T}$. Fractional calculus grew more sophisticated in 2015; Caputo and Fabrizio introduced the Caputo-Fabrizio fractional operator, which includes an exponential and non-singular kernel [11]. That being said, the CF operator is criticized because the CF operator's kernel is non-singular and local and because the operator's solution has the shape of an exponential equation rather than an exponential function. Because of their significant utility in the biological sciences, fractional differential operators present a fresh technique for solving these challenges. Subsequently, Atangana and Baleanu introduced the renowned AB-fractional operator with the Mittag-Leffler non-singular kernel, which yields a limited solution and a stabilising point [12]. Tilak Raj Prabhakar, a renowned mathematician from India, introduced a novel three-parameter fractional derivative operator. This operator is one of the three distinct fractional derivative definitions associated with the Mittag-Leffler function, collectively known as the Prabhakar fractional derivative. Successful applications of classical kernels are reported by this fractional derivative operator with Mittag-Leffer [13]. Atangana has explored the connections between practical computational problems and the concepts of fractal and fractional derivatives. In a previous work, Atangana et al. [14] provided a comprehensive assessment of the recently proposed operators for solving fractal fractional differential equations. Kolsi et al. [15] examined the impact of different nanoparticles using fractional scheme. In [16] authors also examined the influence of various nanomaterial's with heat transfer and fractional approach. Ramesh et al. [17] investigated the numerical solution of Jeffery type hybrid nanofluid. A multi-dimensional chaotic structure lacking an equilibrium position within a fractal-fractional Mittag-Leffler kernel is analyzed mathematically and numerically in Ref. [18–26].

Employing the Prabhakar derivative with precise fractional parameters may be a good strategy for identifying acceptable numerical models that are recognized for achieving a sufficient balance of experimental and imagined results [27,28]. Shah et al. [29] explored a Prabhakar component of the Maxwell fluid model, which included heat transfer and free convection flow. Asjad et al. [30] used the Prabhakar operator to solve the fractional issue of Jeffrey's fluid on a revolving perpendicular plate, along with the energy problems. They used the Laplace approach to derive momentum. Sarwar et al. [31] investigated the convectional velocity of a Casson solvent via a vibrating medium, adopting a Prabhakar fractional technique based on the extended Fourier law. Chen et al. [32] investigated the impact of the slip rate restriction on the flow property of the Oldroyd-B fluid by extrapolating Fick's and Fourier's laws utilizing the Prabhakar fractional function. Basit et al. [33] employed the Prabhakar fractional technique to study the outcome of second-grade fractional nanofluid equipment with numerous kinds of nanoparticles. Samraiz et al. [34] introduce the Hilfer-Prabhakr fractional derivative method addressing mathematical problems. Elnaqeeb et al. [35] have investigated the impression of a viscous liquid using the Prabhakar fractional derivative function. Aiyashi et al. [36] investigated the impact of dense dissipation and generated magnetic fields on unstable mixed turbulent stalling point flows. This shows that the magnetic field produced significantly influenced the study's results. Pandey et al. [37] investigated the magneto-radiative and heating convective motion of boundaries in a Maxwell fluid over a permeable inclination perpendicular plate, taking into account the implications of the generated magnetic field. The research [38] and [39] focused on how generated magnetic fields and heat rays affect the magneto-convection circulation of a dissipative medium. This suggests that the magnetic field that was generated had a key role in these evaluations.Applying Leibniz's derivative to discontinuous fractal media leads naturally to the fractal derivative. It fits the description of a unique localized fractional derivative [40]. The use of the fractal derivative in fractal medium has garnered significant interest. For instance, it can simulate heat transport and water penetration in multi-scale textile and wool fibers [41]. By using numerical techniques, Srivastava et al. [42] have compiled a set of fractional-order system of equations with singularity and severe nonlinear effects related to electrodynamics flow in an annular cylindrical tunnel. Imran [43] has been studying the fractal fractional derivative to explain the basis or flow of viscoelastic fluid. MHD affects flow between two indefinitely long parallel plates. However, the phenomenon of heat transport issue with fluid flow hasn't yet been studied using the novel concept of the fractal-fractional derivative. In recent years, fractal-fractional derivatives and their associated integrals have garnered significant attention due to their wide-ranging applications in modeling a variety of real-world phenomena across diverse domains, such as ecology, finance, medicine, and chemistry [27,44-49].

Many researchers have been interested in the simple problem of a fluid sheared between two parallel plates distanced by a distance H ever since Couette's investigation in 1890. The most alluring aspect of laminar flow is its straightforward flow pattern with a linear velocity profile. This served as the foundation for the explanation of Newton's viscosity law. The classic work of Taylor serves as the foundation for experimental observations using concentric cylinders that resemble true Couette flow between parallel surfaces. This case involved a setup where a porous medium was connected to a fixed plate, and uniform heat fluxes of varying intensities were applied to both plates. The governing equations used to model this system were the Brinkman-Forchheimer-Darcy equations [50]. Furthermore, more recent research on different hybrid nanofluids with different mathematical schemes can see in [51–56].

Turbulent Couette flow has received renewed attention during the last decade or so. Kitoh et al. [57] investigated planar Couette flow with a conveyor belt that ran through a 0.88 m by 5.12 m channel. It is widely known that the Couette-Taylor flow in Newtonian fluids shows a diverse set of oscillations [58]. Liu and Khomami [59] employed the DNS method to describe the flow of a polymer mixture in a Taylor-Couette apparatus. An analysis of a section of the published work reveals a lack of an acceptable analytical or semi-analytical approach to analyze its stability and instability, as well as the problem's velocity pattern [60]. They investigated a solution to the erratic MHD Couette flow issue

with an exterior with flexibility made up of two convergent porous tubes with infinite lengths and fluid generated by the impulsive or increased initiatives of the outer pistons, witnessing that injection results in flow a delay while suctions cause flow rapidity. The polymer-induced splitting of large Taylor swirled into fewer of them, considerably enhancing drag forces near the walls. Eskin [61] identified a laboratory Couette device as a viable tool for studying drag-reducing chemicals because of the resemblances between Couette and pipe flow structures.

To the best of the author's knowledge, no attempt has been made to investigate the unsteady Jeffrey-type Hybrid nanofluid flow of fundamental fluxes under the impact of magnetic field and inclination. We explored the basic and modified Couette flows of an MHD volatile Jeffrey-type hybrid nanofluid using an inclined microchannel in this work. We used the two most current and modified definitions of fractional derivatives, Prabhakar and Fractal non-integer order derivatives. We also employed the integral transform, particularly the Laplace transformation, to cope with the governed non-dimensional PDEs solution. In all instances, velocity profile solutions are derived using numerical methodologies such as the Stehfest and Tzous algorithms. To study vertical channel data, set $\wp = \pi/2$, and to gather horizontal channel results, set $\wp = 0$. The search outcomes show that hybrid nanofluids have better thermal transfer capacities than typical fluids in addition to single-nanoparticle nanofluids. This is because of the collective effect of the several nanostructures in the hybrid composition. The chemical structure and quantity of the hybrid nanoparticles may be adjusted to improve the nanofluid's thermophysical features, such as heat electrical conductivity, thickness, and weight, for specific uses. Hybrid nanofluids can boost the effectiveness and output of energy sources, including solar thermal enthusiasts, nuclear-powered reactors, and power plants. These are the most common issues. Finally, graphics show the influence of the major factors on flow quantities.

Nomenclature:

Symbol		Quantity	Unit
T_d	:	Ambient temperature	(K)
$\wp$	:	The angle of magnetic inclination	$(-)$
U_0	:	Characteristic velocity	(ms^{-1})
q	:	Laplace transform variable	$(-)$
μ_{nf}	:	Dynamic viscosity	(Kg/ms)
σ	:	Electrical Conductivity	$(-)$
$\wp$	:	Fluid velocity	(m/s)
α, β	:	Fractional parameters	$(-)$
Gr	:	Heat Grashof number	$(-)$
Gm	:	Mass Grashof number	$(-)$
M	:	Magnetic field	$(-)$
ρ_{nf}	:	Nano-fluid density	(Kg/m^3)
Nu	:	Nusselt number	$(-)$
B_o	:	Strength of Magnetic field	(Kg/s^2)
g	:	Gravity acceleration	(m/s^2)
Sh	:	Sherwood number	$(-)$
C_p	:	Specific heat at the constant pressure	(J/kgK)
Sc	:	Schmidt number	$(-)$
C_f	:	Skin friction	$(-)$
$\wr$	:	Times	(s)
k_{nf}	:	Thermal Conductivity of the Nanofluid	(W/mk)
β_T	:	Thermal expansion coefficient	$(1/k)$
T_w	:	Wall temperature	(K)

2. Formulations of governed equations

This article describes a Jeffery-type hybrid nanofluid free convection that passes via two hot side plates positioned in the *xy*-plane and *h*-distance apart in a rectangular coordinate system. For the moving hybrid nanofluid, several nanoparticles ($Ag + TiO_2$) are considered mixed in ($H_2O, C_6H_9NaO_7$) as the base fluids. This flow passes through an inclined material with a uniform density while an inclined magnetic field is present. At a set point temperature T_0, the whole system—which comprises the fluid and its constraints—remains in its original equilibrium. When time-dependent shear force is applied, the upper plate ($y = h$)

begins to move in its plane at time $t > 0$. Owing to the pressure gradient, temperature field augmentation, and oscillation, the static hybrid nanofluid begins to flow through the inclined channel. The following considerations are put forth to help formulate regulated PDEs.

- The microchannel has an unlimited length and a width of *h*.
- The microchannel oscillates perpendicular to the y-axis and along the x-axis.
- The leading equations are developed for incompressible fluid flow when density (ρ) is fixed and devoid of time and distance.
- This simplifies the continuity equation to the incompressibility assumption ($\nabla \cdot u = 0$).
- The system's temperature is T_0 at time $t = 0$.
- The temperature rises from T_0 to T_w after $t > 0$.
- Modifications in the heat field and pressure disparity cause fluid to travel faster in the x direction.
- An inclined magnetic field ($\wp$) with a B_0 intensity operates against the flow direction.
- During flow rates, inertial effects must be addressed, and expanded Darcy equations are more applicable.

An in-compressible MHD Jeffrey-type hybrid nanofluid over the inclined plane can be assessed using the following PDE governing system [17]

$$\nabla \cdot \overline{\mathscr{S}} = 0 \tag{1}$$

$$\rho \left(\frac{\partial \overline{\mathscr{S}}}{\partial \mathfrak{I}} + \overline{\mathscr{S}} \cdot \nabla \overline{\mathscr{S}} \right) = -\nabla p + \nabla \cdot \overline{\mathbb{S}} + \overline{\mathfrak{R}} + \overline{\mathscr{J}} \times \mathscr{B} \tag{2}$$

here $\overline{\mathscr{S}}$, ρ, $\mathfrak{I}$, p, $\overline{\mathbb{S}}$, $\overline{\mathfrak{R}}$, $\overline{\mathscr{J}}$, and $\overline{\mathscr{B}}$, signifying the velocity vector, time, pressure, stress tensor, Darcy's resistance, current vector, and magnetic field intensity. Where

$$\overline{\mathfrak{R}} = -\frac{\mu}{k} \overline{\mathscr{S}}, \overline{\mathbb{S}} = \frac{\mu}{1+\lambda} (\dot{r} + \lambda_o \ddot{r}), \overline{\mathscr{J}} = \sigma(\overline{E} + \overline{q} \times \mathscr{B}), \dot{r} = \nabla \overline{\mathscr{S}} + (\nabla \overline{\mathscr{S}})^T$$

$$\ddot{r} = \frac{d\dot{r}}{dt} = \frac{\partial \dot{r}}{\partial t} + (\overline{\mathscr{S}} \cdot \nabla)\dot{r}$$

are the mathematical forms of the above-defined constraints.

From the above assumptions, the governed PDE of this inclined flow will be modeled for the Jeffrey-type hybrid nanofluid [62,63]

$$\frac{\partial \wp(Y, \mathfrak{I})}{\partial \mathfrak{I}} = -\frac{\partial \overline{\mathfrak{R}}}{\partial x} + \frac{1}{\rho_{hnf}} \frac{\mu_{hnf}}{(1+\Lambda)} \left(\frac{\partial^2 \wp(Y, \mathfrak{I})}{\partial Y^2} \right) + g \sin(\wp)$$
$$- \frac{\sigma_{hnf}}{\rho_{hnf}} B_0^2 \sin(\wp) \wp(Y, \mathfrak{I}) - \frac{\mu_{hnf}}{\rho_{hnf}} \frac{1}{k} \wp(Y, \mathfrak{I}) \tag{3}$$

Where μ_{hnf}, k and ρ_{hnf} are the coefficients of viscosity, porosity, and density of the hybrid nanofluid. σ_{hnf} are the electrical conductivity and β_0 intensity of the magnetic field. And Λ is the relation of retardation and relaxation time, and $\frac{\partial \overline{\mathfrak{R}}}{\partial x}$ is the pressure gradient.

3. Solution of fundamental flow

In this part of the study, the controlled partial differential equation (PDE) solution is evaluated through the application of two distinct and recently developed fractional derivative definitions, namely the fractal fractional derivative and the Prabhakar fractional derivative. Furthermore, the Laplace transform integral transform approach is employed to obtain the solutions for both the simple and generalized Couette flow cases, following the non-dimensionalization of the governing equations.

3.1. Simple Couette flow by FFD

In an applied inclination magnetic field, we examined an unsteady

and incompressible MHD Jeffrey fluid flowing across an inclined microchannel separated by *h*. The top plate vibration and temperature fluctuation cause the Jeffery-type hybrid nanofluid containing $(C_6H_9NaO_7 + Ag + TiO_2)$ and $(H_2O + Ag + TiO_2)$ hybrid nanofluids to circulate. As seen in Fig. 1, the fluid movement happens horizontally as a result of the top plate vibrating.

Considering these presumptions in place, the leading equation may be expressed as

$$Re\,^{FFD}\mathfrak{D}_t^{\alpha,\beta}\wp(Y,\ell) = \beta\ell^{\beta-1}\left[\Lambda_1\frac{\partial^2\wp(Y,\ell)}{\partial Y^2} - \frac{1}{D_a}\wp(Y,\ell) - \mathscr{M}^2 sin(\mathscr{g})\wp(Y,\ell) + \frac{Re}{Fr}sin(\wp)\right] - \frac{\wp(Y,0)}{\Gamma(1-\alpha)}\ell^{-\alpha} \tag{12}$$

$$\frac{\partial\wp(Y,\mathfrak{J})}{\partial\mathfrak{J}} = \frac{1}{\rho_{hnf}}\frac{\mu_{hnf}}{(1+\Lambda)}\left(\frac{\partial^2\wp(Y,\mathfrak{J})}{\partial Y^2}\right) + g\,sin(\wp) - \frac{\sigma_{hnf}}{\rho_{hnf}}B_0^2 sin(\mathscr{g})\wp(Y,\mathfrak{J})$$
$$- \frac{\mu_{hnf}}{\rho_{hnf}\,k}\frac{1}{k}\wp(Y,\mathfrak{J}) \tag{4}$$

With corresponding conditions

$$\wp(0,\mathfrak{J}) = 0;\ \forall\,\mathfrak{J} \tag{5}$$

$$\wp(h,\mathfrak{J}) = U_a\mathscr{f}(t);\ \mathfrak{J} > 0 \tag{6}$$

$$\wp(Y,0) = 0;\ 0 \le Y < h \tag{7}$$

Presenting the non-dimensional quantities

$$\overline{Y} = \frac{Y}{l},\ \overline{\wp} = \frac{\wp}{U_o},\ D_a = \frac{k'}{l^2},\ R_e = \frac{\rho U_o l}{\mu},\ \overline{\ell} = \frac{U_o\mathfrak{J}}{l},\ \overline{h} = \frac{h}{l},$$

$$Fr = \frac{U^2}{gl},\ \mathscr{M} = \sqrt{\frac{\sigma}{\mu}}\beta_0 l,\ \Lambda_1 = \frac{1}{(1+\Lambda)}$$

After using above constraints and neglecting the bar notation, we yield

$$Re\frac{\partial\wp(Y,\ell)}{\partial\ell} = \frac{Re}{Fr}sin(\wp) + \Lambda_1\frac{\partial^2\wp(Y,\ell)}{\partial Y^2} - \frac{1}{D_a}\wp(Y,\ell) - \mathscr{M}^2 sin(\mathscr{g})\wp(Y,\ell) \tag{8}$$

With it corresponding dimensionless conditions

$$\wp(0,\ell) = 0;\ \forall\,\ell \tag{9}$$

$$\wp(h,\ell) = \mathscr{f}(t);\ \ell > 0 \tag{10}$$

$$\wp(Y,0) = 0;\ 0 \le Y < h \tag{11}$$

3.1.1. Solution of Couette flow by FFD definition

Using the above non-dimensional constraints and also utilizing the definition of fractal fractional derivative definition, we attain the second order PDE for simple couette flow

With dimensionless conditions

$$\wp(0,\ell) = 0;\ \forall\,\ell \tag{9a}$$

$$\wp(h,\ell) = \mathscr{f}(t);\ \ell > 0 \tag{10a}$$

$$\wp(Y,0) = 0;\ 0 \le Y < h \tag{11a}$$

It is a more convenient approach to apply the Laplace transform (LT) on the governing partial differential equation (PDE) for the simple Couette flow problem. By employing the Laplace transform on the PDE for simple Couette flow, along with the corresponding Laplace definition of the fractal fractional derivative (FFD) and the associated boundary conditions, the solution for the momentum field in the simple Couette flow can be obtained.

$$\overline{\wp}(Y,q) = \frac{\mathfrak{h}_8}{(\mathfrak{h}_2 + \mathfrak{h}_6 q^{\alpha+\beta})}\left(1 - \frac{sinh\left(Y\sqrt{\mathfrak{h}_3 + \mathfrak{h}_4 q^{\alpha+\beta}}\right)}{sinh\sqrt{(\mathfrak{h}_3 + \mathfrak{h}_4 q^{\alpha+\beta})}}\right)$$
$$+ \mathscr{F}(q)\frac{sinh\left(Y\sqrt{\mathfrak{h}_3 + \mathfrak{h}_4 q^{\alpha+\beta}}\right)}{sinh\sqrt{(\mathfrak{h}_3 + \mathfrak{h}_4 q^{\alpha+\beta})}} \tag{13}$$

where:

$$\mathfrak{h}_1 = \mathscr{M}^2 sin(\mathscr{g}),\ \mathfrak{h}_2 = \mathfrak{h}_1 + \frac{1}{D_a},\ \mathfrak{h}_3 = \frac{\mathfrak{h}_2}{\Lambda_1},\ \mathfrak{h}_4 = \frac{Re}{\Lambda_1\,\beta\,\Gamma(\beta)},$$

$$\mathfrak{h}_5 = sin(\wp),\ \mathfrak{h}_6 = \frac{Re}{\beta\,\Gamma(\beta)},\ \mathfrak{h}_7 = \frac{Re}{Fr},\ \mathfrak{h}_8 = \mathfrak{h}_5 * \mathfrak{h}_7$$

3.1.2. Solution of Couette flow by PFD definition

For the solution in the sense of Prabhakar fractional derivative,
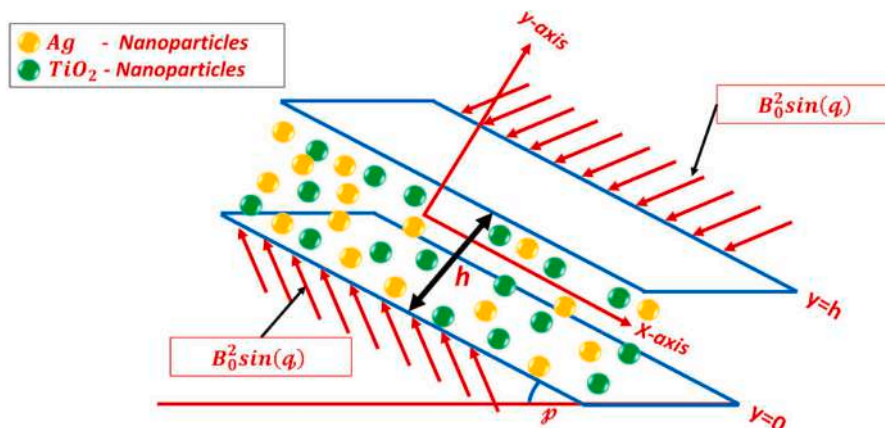
Fig. 1. Geometry of simple Couette flow.

retaining the definition of Prabhakar fractional integral and using the time derivative in the sense of Prabhakar fractional derivative operator, we get.

$$R_e^{PFD}\mathfrak{D}_t^{\alpha,\beta,\gamma}\mathscr{e}(Y,\mathscr{t}) = \frac{Re}{Fr}sin(\mathscr{r}) + \Lambda_1\frac{\partial^2\mathscr{e}(Y,\mathscr{t})}{\partial Y^2} - \frac{1}{D_a}\mathscr{e}(Y,\mathscr{t}) - \mathscr{M}^2sin(\mathscr{g})\mathscr{e}(Y,\mathscr{t})$$

(14)

With the same initial and boundary conditions as like for the solution of FFD section. Now by retaining the LT on the above Eq. (14)

$$\frac{\partial^2\overline{\mathscr{e}}(Y,q)}{\partial Y^2} - \frac{1}{\Lambda_1}\left(\frac{1}{D_a}+\mathscr{M}^2sin(\mathscr{g})+q^\beta(1-\alpha q^{-\alpha})^\gamma\right)\overline{\mathscr{e}}(Y,q) + \frac{Re}{Fr}sin(\mathscr{r}) = 0$$

$$\overline{\mathscr{e}}(0,q) = 0; \quad \overline{\mathscr{e}}(h,q) = \mathscr{F}(q); \quad \overline{\mathscr{e}}(Y,0) = 0$$

By solving the above second-order differential equation with its correspondence boundary conditions

$$\overline{\mathscr{e}}(Y,q) = \frac{\mathfrak{h}_8}{(\mathscr{y}_1 + Re\ q^\beta(1-\alpha q^{-\alpha})^\gamma)}\left(1 - \frac{sinh\left(Y\sqrt{\mathscr{y}_2 + \mathscr{y}_3\ q^\beta(1-\alpha q^{-\alpha})^\gamma}\right)}{sinh\sqrt{(\mathscr{y}_2 + \mathscr{y}_3\ q^\beta(1-\alpha q^{-\alpha})^\gamma)}}\right)$$
$$+ \mathscr{F}(q)\frac{sinh\left(Y\sqrt{\mathscr{y}_2 + \mathscr{y}_3\ q^\beta(1-\alpha q^{-\alpha})^\gamma}\right)}{sinh\sqrt{(\mathscr{y}_2 + \mathscr{y}_3\ q^\beta(1-\alpha q^{-\alpha})^\gamma)}}$$

(15)

Where:

$$\mathscr{y}_1 = \mathscr{M}^2sin(\mathscr{g}) + \frac{1}{D_a}, \quad \mathscr{y}_2 = \frac{\mathscr{y}_1}{\Lambda_1}, \quad \mathscr{y}_3 = \frac{Re}{\Lambda_1}, \quad \mathfrak{h}_8 = \mathfrak{h}_5 * \mathfrak{h}_7$$

3.2. Generalized Couette flow

In this study, the focus is on the unsteady and incompressible mag-

netohydrodynamic (MHD) Jeffrey-type hybrid nanofluid flow between two horizontal, inclined parallel plates separated by a distance *h*. Similar to the simple Couette flow configuration, the entire system is initially at a constant state. After some time, due to the variation in thermal profile and pressure gradient $\mathscr{H} = -\frac{\partial \mathfrak{R}}{\partial x}$, the static fluid starts to move through the microchannel. This condition is analogous to the Couette flow. It is presumed that the bottom plate is at a constant position, and the top plate is moving at a perpetual velocity U_o, as shown in Fig 2.

With the hypotheses, the equation regulating the flow may be expressed as for generalized Couette flow

$$\frac{\partial\mathscr{e}(Y,\mathfrak{I})}{\partial\mathfrak{I}} = \mathscr{H} + \frac{1}{\rho_{hnf}}\frac{\mu_{hnf}}{(1+\Lambda)}\left(\frac{\partial^2\mathscr{e}(Y,\mathfrak{I})}{\partial Y^2}\right) + g\ sin(\mathscr{r})$$
$$- \frac{\sigma_{hnf}}{\rho_{hnf}}B_0^2sin(\mathscr{g})\mathscr{e}(Y,\mathfrak{I}) - \frac{\mu_{hnf}}{\rho_{hnf}}\frac{1}{k}\mathscr{e}(Y,\mathfrak{I})$$

(16)

$$\mathscr{e}(0,\mathfrak{I}) = 0; \quad \mathscr{e}(h,\mathfrak{I}) = U_o\mathscr{f}(t); \quad \mathscr{e}(Y,0) = 0$$

Familiarizing the non-dimensional quantities

$$\overline{Y} = \frac{Y}{l}, \quad \overline{\mathscr{e}} = \frac{\mathscr{e}}{U_o}, \quad D_a = \frac{k'}{l^2}, \quad R_e = \frac{\rho U_o l}{\mu}, \quad \overline{\mathfrak{I}} = \frac{U_o\mathfrak{I}}{l}, \quad \overline{h} = \frac{h}{l}, \quad \mathscr{M} = \sqrt{\frac{\sigma}{\mu}}\beta_0 l, \quad \overline{\mathscr{H}}$$
$$= \frac{l^2 G}{\mu U_o}$$

Using the above parameters

$$R_e\frac{\partial\mathscr{e}(Y,\mathscr{t})}{\partial\mathscr{t}} = \mathscr{H} + \Lambda_1\frac{\partial^2\mathscr{e}(Y,\mathscr{t})}{\partial Y^2} - \frac{1}{D_a}\mathscr{e}(Y,\mathscr{t}) - \mathscr{M}^2sin(\mathscr{g})\mathscr{e}(Y,\mathscr{t}) + \frac{Re}{Fr}sin(\mathscr{r})$$

(17)

and dimensionless initial and boundary conditions are

$$\mathscr{e}(0,\mathscr{t}) = 0; \quad \mathscr{e}(h,\mathscr{t}) = \mathscr{f}(t); \quad \mathscr{e}(Y,0) = 0$$

3.2.1. Solution of generalized Couette flow by FFD definition

For the finite solution of the above-considered PDE, utilizing the definition of FFD integral and its corresponding derivative operator, we have

$$^{FFD}\mathfrak{D}_t^{\alpha,\beta}$$

$$\mathscr{e}(Y,\mathscr{t}) = \beta\mathscr{t}^{\beta-1}\left[\frac{\mathscr{H}}{R_e}+\frac{\Lambda_1}{R_e}\frac{\partial^2\mathscr{e}(Y,\mathscr{t})}{\partial Y^2} - \frac{1}{R_e\ D_a}\mathscr{e}(Y,\mathscr{t}) - \frac{\mathscr{M}^2}{R_e}sin(\mathscr{g})\mathscr{e}(Y,\mathscr{t}) + \frac{1}{Fr}sin(\mathscr{r})\right] - \frac{\mathscr{e}(Y,0)}{\Gamma(1-\alpha)}\mathscr{t}^{-\alpha}$$

By using the LT with its boundary conditions, we get the generalized velocity profile as follows

$$\overline{\mathscr{e}}(0,q) = 0; \quad \overline{\mathscr{e}}(h,q) = \mathscr{F}(q); \quad \overline{\mathscr{e}}(Y,0) = 0$$

and

Fig. 2. Geometry of Generalized Couette flow.

$$\overline{\nu}(Y, q) = \frac{\mathscr{H}}{\mathfrak{h}_2 + \mathfrak{h}_6 q^{\alpha+\beta}} \left(1 - \frac{\sinh\left(y\sqrt{\mathfrak{h}_3 + \mathfrak{h}_4 q^{\alpha+\beta}}\right)}{\sinh\sqrt{(\mathfrak{h}_3 + \mathfrak{h}_4 q^{\alpha+\beta})}}\right)$$

$$+ \frac{\mathfrak{h}_8}{(\mathfrak{h}_2 + \mathfrak{h}_6 q^{\alpha+\beta})} \left(1 - \frac{\sinh\left(Y\sqrt{\mathfrak{h}_3 + \mathfrak{h}_4 q^{\alpha+\beta}}\right)}{\sinh\sqrt{(\mathfrak{h}_3 + \mathfrak{h}_4 q^{\alpha+\beta})}}\right)$$

$$+ \mathscr{F}(q)\frac{\sinh\left(Y\sqrt{\mathfrak{h}_3 + \mathfrak{h}_4 q^{\alpha+\beta}}\right)}{\sinh\sqrt{(\mathfrak{h}_3 + \mathfrak{h}_4 q^{\alpha+\beta})}} \qquad (18)$$

3.2.2. Solution of generalized Couette flow by PFD definition

For the solution in the sense of Prabhakar fractional derivative, using PFD operator on Eq. (17).

$$R_e \, ^{PFD}\mathfrak{D}_t^{\alpha,\beta,\gamma}$$

$$\nu(Y, \ell) = \mathscr{H} + \Lambda_1 \frac{\partial^2 \nu(Y, \ell)}{\partial Y^2} - \frac{1}{D_a}\nu(Y, \ell) - \mathscr{M}^2 \sin(\mathcal{G})\nu(Y, \ell) + \frac{Re}{Fr}\sin(\nu)$$

Again employing the Laplace transformation on the above transformed equation and on boundary conditions

$$\frac{\partial^2 \overline{\nu}(Y, q)}{\partial Y^2} = \frac{\mathscr{M}^2}{\Lambda_1}\sin(\mathcal{G})\overline{\nu}(Y, q) - \mathscr{H} - \frac{Re}{Fr}\sin(\nu) + \frac{1}{\Lambda_1}q^\beta(1 - \alpha q^{-\alpha})^\gamma \overline{\nu}(Y, q)$$

$$+ \frac{1}{\Lambda_1}\frac{1}{D_a}\overline{\nu}(Y, q) \qquad (19)$$

$$\overline{\nu}(0, q) = 0; \; \overline{\nu}(h, q) = \mathscr{F}(q); \; \overline{\nu}(Y, 0) = 0$$

After using the above boundary conditions, the solution of the above nonhomogeneous differential equation will become as follows

$$\overline{\nu}(Y, q) = \frac{\mathscr{H}}{\mathfrak{h}_2 + \mathfrak{h}_6 \, \mathfrak{U}_2}\left(1 - \frac{\sinh(y\sqrt{\mathfrak{U}_4})}{\sinh(\sqrt{\mathfrak{U}_4})}\right)$$

$$+ \frac{\mathfrak{h}_8}{(\mathcal{Y}_1 + Re \, \mathfrak{U}_2)}\left(1 - \frac{\sinh(y\sqrt{\mathfrak{U}_4})}{\sinh(\sqrt{\mathfrak{U}_4})}\right) + \mathscr{F}(q)\frac{\sinh(y\sqrt{\mathfrak{U}_4})}{\sinh(\sqrt{\mathfrak{U}_4})} \qquad (20)$$

Where:

$$\mathfrak{U}_1 = 1 - \alpha q^{-\alpha}, \; \mathfrak{U}_2 = q^\beta \mathfrak{U}_1^\gamma, \; \mathfrak{U}_3 = \mathfrak{h}_4 \mathfrak{U}_2, \; \mathfrak{U}_4 = \mathfrak{h}_3 + \mathfrak{U}_3$$

Several researchers have employed various numerical methods to obtain the Laplace inverse of the solutions to the governing equations [64–66]. Since the solutions for the basic Couette flow and the generalized Couette flow are more complex, numerical techniques, specifically the Stehfest algorithm and Tzou's approach, were utilized in this study. The mathematical formulations of these numerical methods are as follows:

$$U(y, t) = \frac{\ln(2)}{t}\sum_{i=1}^{\infty} C_k \overline{U}\left(y, k\frac{\ln(2)}{t}\right)$$

$$C_k = (-1)^{k+p}\sum_{j=\frac{k+1}{2}}^{min(k,p)}\frac{j^p(2j)!}{(p-j)!j!(i-1)!(k-1)!(2i-k)!}$$

$$U(y, t) = \frac{e^{4.7}}{t}\left[0.5\overline{U}\left(y, \frac{4.7}{t}\right) + Re\left\{\sum_{l=1}^{M}(-1)^l \overline{U}\left(y, \frac{4.7 + l\pi i}{t}\right)\right\}\right]$$

Validity and Comparison:

This section assesses the validity, compares results, and discusses the consequences of the Prabhakar and Fractal fractional schemes on hybrid nanofluids. To validate the findings of this investigation, the finalized velocity profile is visually compared with the outcomes measured by Ramesh et al. [17] in Fig. 4a and b. The combination of curves verifies this research. The resemblance of curves gives concrete evidence for the study's validity. This validation reinforces the theoretical foundation upon which the research is based. The Fig. 3a and b were plotted to validate the numerical techniques used, specifically the Stehfest and Tzou's algorithms. The overlapping nature of the curves for both the simple and generalized Couette flow situations indicates that the obtained results and the numerical techniques employed have been successfully validated. Subsequently, as with this work, we investigated a Jeffery-type hybrid nanofluid passing via an inclined channel. Fig. 5a and b provide graphical representations of the hybrid nanofluids under consideration for various time values. The influence of $(C_6H_9NaO_7 + Ag + TiO_2)$-based hybrid nanofluid on the forward motion field is somewhat more significant than that of $(H_2O + Ag + TiO_2)$ based hybrid nanofluid for both Couette flow and generalized flow at small time scales. As time passes, the velocity profile grows exponentially and diverges in direction, and the effect of $(H_2O + Ag + TiO_2)$-based hybrid nanofluid grows stronger than that of $(C_6H_9NaO_7 + Ag + TiO_2)$-based hybrid nanofluid, as seen in the figures.

4. Explanation of results

In this work, we evaluated the Jeffery-type hybrid nanofluid containing $(C_6H_9NaO_7, H_2O)$ base fluid and (TiO_2, Ag) nanoparticles. The Jeffrey fluid model is a non-Newtonian fluid with viscoelastic dynamics and an exclusive memory time continuum known as the relaxation period time. Jeffrey fluid models are used to analyze both the thermal and flow properties of nanofluids. To summarize, the $(Cu - Ag/H_2O - C_2H_6O_2)$ hybrid nanofluid is a special type of Jeffrey nanofluid. The flow pattern is analyzed for two scenarios: basic Couette flow and generalized Couette flow over an angled microchannel. The magnetic field from the outside is also used to regulate the speed of fluids. The non-dimensionalized governed PDEs are converted using the most current fractional definitions, Fractal and Prabhakar fractional derivatives, and then empirically solved via the Laplace transformation. Figs. 3-5 provide a detailed discussion of the obtained results' validity and graphical comparison analysis. Furthermore, Figs. 6-13 examine the physical influence of various limitations on fluid velocity for both types of fluids. Fig. 6 (a-d) demonstrate the influence of fractional constraints α, β, γ
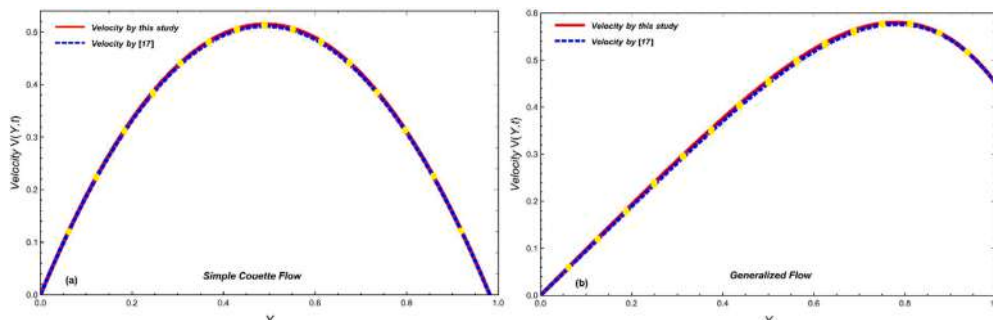
Fig. 3. Comparison of this study with Ramesh et al. [17].
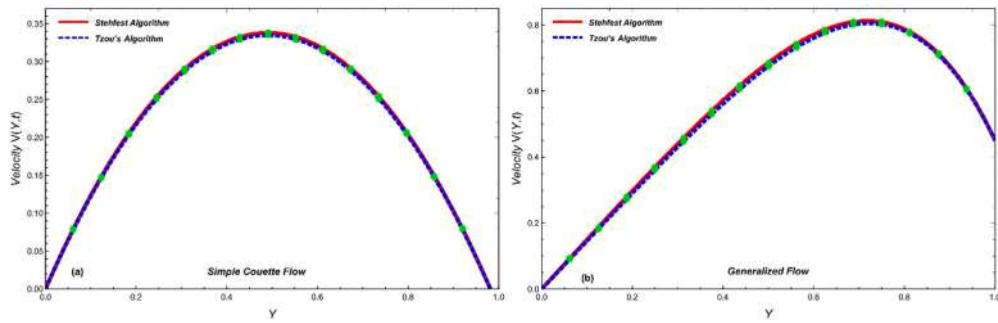
Fig. 4. Comparison of numerical algorithms.
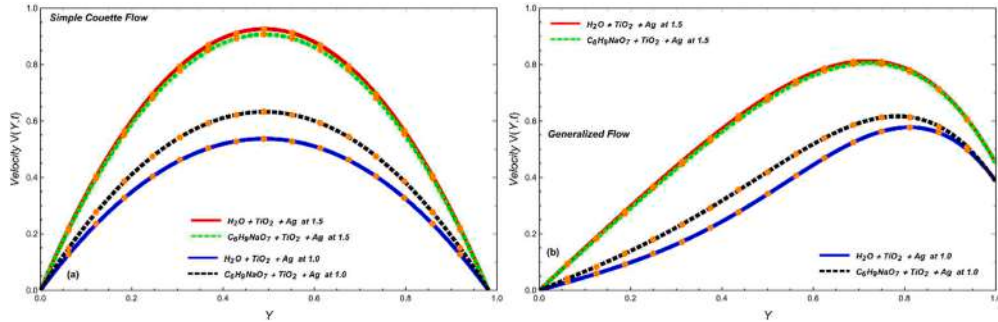
Fig. 5. Comparison of considered base fluids.
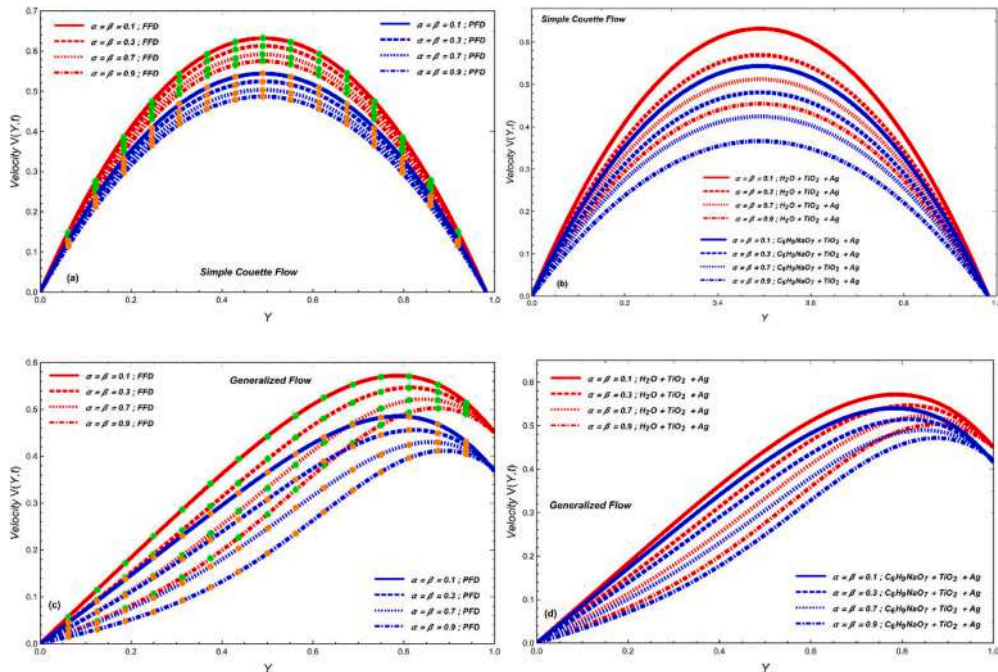
Fig. 6. Influence of α, β on $\ell(Y, \ell)$ with $\gamma = 0.7$, $Re = 0.6$, $\mathscr{g} = \frac{\pi}{4}$, $M = 2.4$, $Fr = 5.2$, $\Lambda_1 = 1.5$, $\ell = 1.4$, $D_a = 0.3$, $\varphi = 0.04$.

with simple and generalized couette flows using various (H_2O) and ($C_6H_9NaO_7$) nanofluids. Fractional attributes are more successful at capturing the viscoelastic character of fluids than integer-order derivatives. In Couette and modified Couette flow, when a fluid is enclosed within two parallel plates that move relative to one another, fractional factors can cause complicated viscoelastic reactions like shear dispersion or hardening. In the context of Couette flow, the incorporation of fractional factors can lead to anomalous transport behavior, resulting in sub-diffusion, where particles or substances exhibit slower movement compared to classical diffusion. Furthermore, when comparing the investigated hybrid nanofluids, the water-based ($H_2O + Ag + TiO_2$) hybrid nanofluid was found to have a slightly more pronounced effect on both the basic and generalized Couette flow velocity profiles, compared to the ($C_6H_9NaO_7 + CU + TiO_2$)-based hybrid nanofluid.

Fig. 7 (a-d) show the effect of D_a on the Jeffery-type nanofluid for simple and generalized Couette flows, accordingly. In fluid science, the Darcy factor represents the relationship between the barrier of friction in a channel and speed of flow across the substrate. The Darcy friction
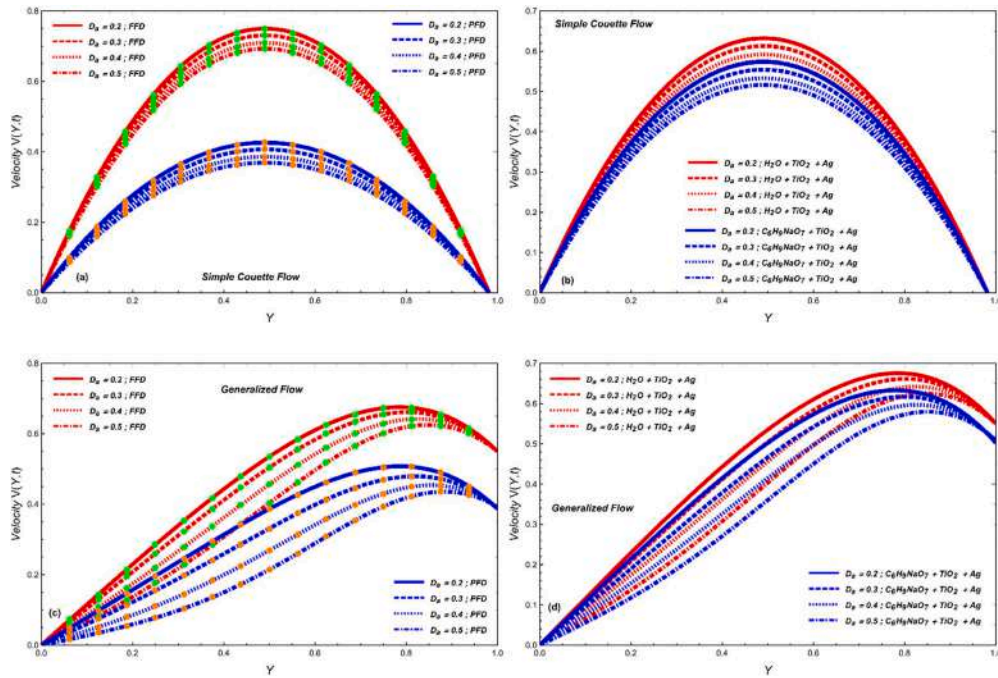
Fig. 7. Influence of D_a on $\ell(Y, \ell)$ with $\alpha = \beta = \gamma = 0.7$, $Re = 0.6$, $g = \frac{\pi}{4}$, $M = 2.4$, $Fr = 5.2$, $\Lambda_1 = 1.5$, $\ell = 1.4$, $\varphi = 0.04$.
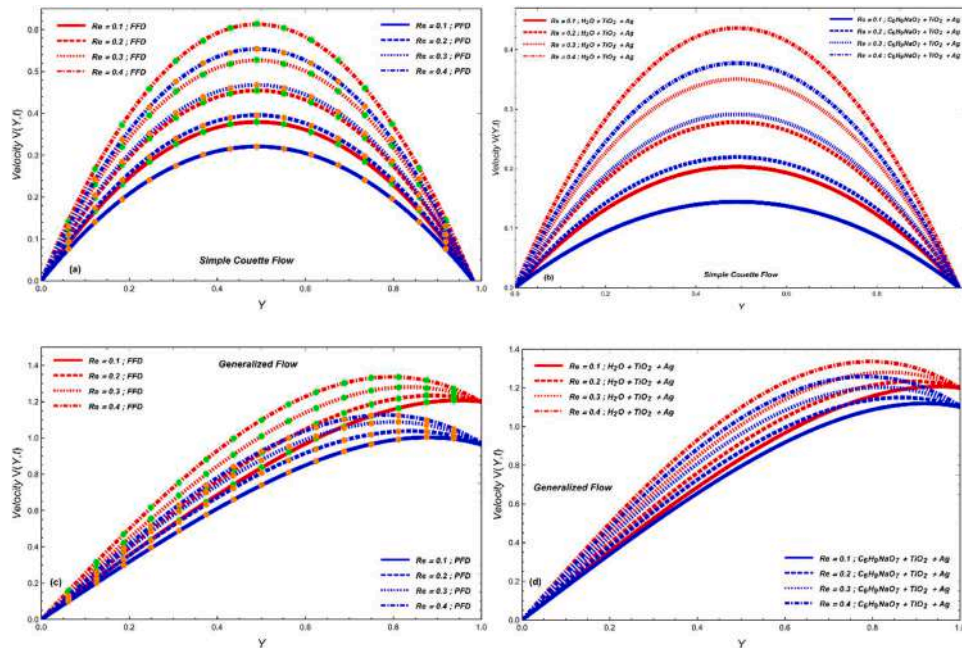
Fig. 8. Influence of Re on $\ell(Y, \ell)$ with $\alpha = \beta = \gamma = 0.7$, $g = \frac{\pi}{4}$, $M = 2.4$, $Fr = 5.2$, $\Lambda_1 = 1.5$, $\ell = 1.4$, $D_a = 0.3$, $\varphi = 0.04$.

factor D_a is associated with the Darcy-Weisbach equation, which describes how friction reduces pressure in an object. It takes into account pipe dimensions, width, fluid acceleration, and resistance. The Darcy number D_a affects the equilibrium of viscous and flexible forces. At moderate Darcy numbers, when buoyant forces are dominant, the patterns of flow may be similar to that of a Newtonian fluid. Conversely, as the Darcy number grows, the flow may display either shear-weakened or shear-thickening conduct according to the fluid's unique rheological characteristics. The Darcy number D_a scientifically defines the percentage of frictional to inertial impacts in a flowing fluid; hence, the D_a parameter causes the fluid speed to drop. Furthermore, like the influence of fractional constraints, the impact of ($H_2O + Ag + TiO_2$) hybrid

nanofluid is bit more as compared to the ($C_6H_9NaO_7 + Ag + TiO_2$) suspension due to the physical significance of considered nanoparticles. The reason for the hybrid nanofluid property modeling may be explored in a variety of settings with various traits such as thermal conductivity, viscosity, specific heat capacity, and nanoparticle attributes. The heat conductivity of hybrid nanofluids is determined by a number of parameters, including the nature and quantity of nanoparticles, the base fluid's characteristics, and the way it interacts with the nanoparticles.

Fig. 8 (a-d) provide a full description of Reynolds number (Re). Reynolds number is a non-dimensional metric used in fluids research to assess a substance's flow. It is defined as the percentage of forces of attraction to viscous forces. The differences in Reynolds number in the
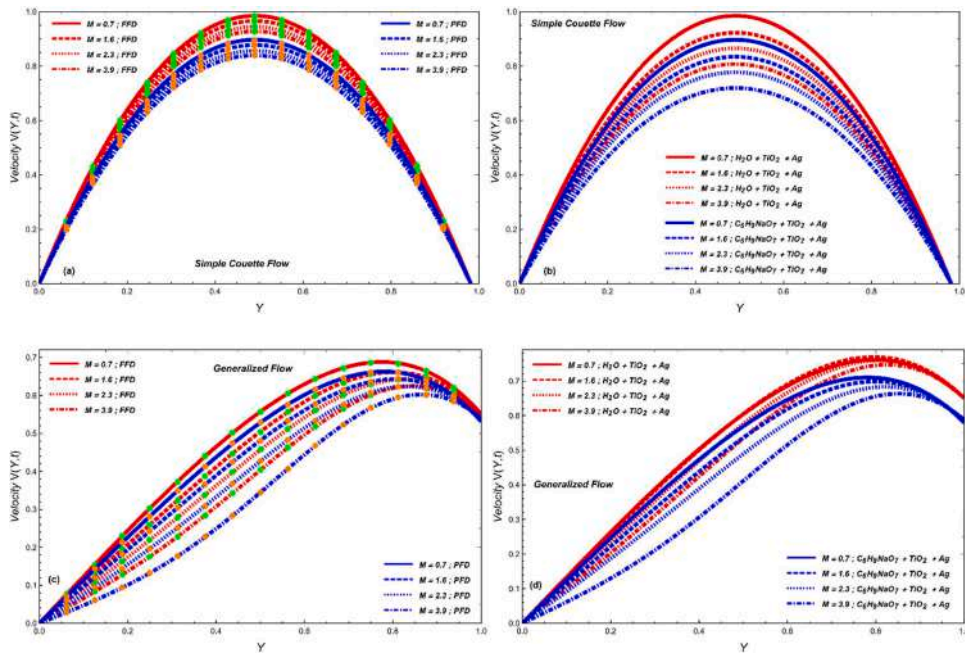
Fig. 9. Influence of M on $\ell(Y, \ell)$ with $\alpha = \beta = \gamma = 0.7$, $Re = 0.6$, $\mathscr{g} = \frac{\pi}{4}$, $Fr = 5.2$, $\Lambda_1 = 1.5$, $\ell = 1.4$, $D_a = 0.3$, $\varphi = 0.04$.
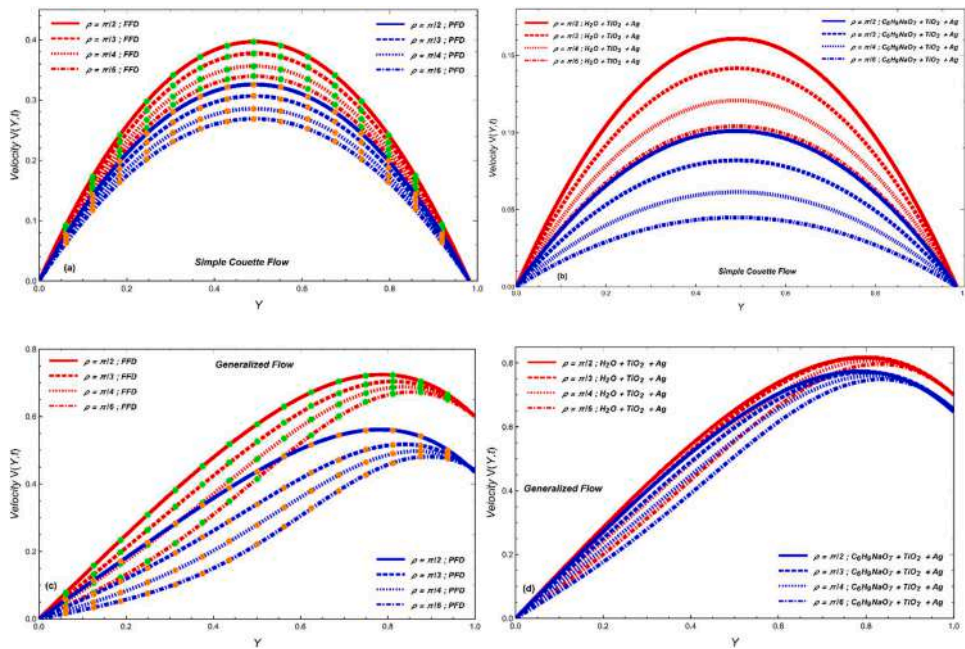
Fig. 10. Influence of $\mathscr{g}$ on $\ell(Y, \ell)$ with $\alpha = \beta = \gamma = 0.7$, $Re = 0.6$, $M = 2.4$, $Fr = 5.2$, $\Lambda_1 = 1.5$, $\ell = 1.4$, $D_a = 0.3$, $\varphi = 0.04$.

turbulent range might not exhibit a straight linear relationship with fluid velocity because other factors, including loss of energy and flow structure, take dominance. The flow pattern can change from laminar to turbulent at a certain Reynolds number. In a turbulence situation, fluid velocity develops extremely irregular and turbulent. Turbulence is distinguished by whirling swirling and momentum variations, which result in improved combining and transfer qualities. The fluid flow may be regulated by varying the (Re) number for both primary and generalized Couette flow.

Figs. 9 and 10 show how the applied ambient magnetic field (M) and the inclination ($\mathscr{g}$) affect each other on the simple and generalized Couette flow. When an electromagnetic field is introduced to a carrying fluid, the reaction of the magnetic field with the fluid's chargeable

particles can drastically alter the flow patterns. This is also referred to as magnetohydrodynamics (MHD). The Lorentz force, which results from the interactions of the magnetic field and the fluid's electrical density, can operate as an extra operating or resistive force in MHD circulation, relying on the relative direction of the magnetic region and the fluid motion. The Lorentz force may influence the velocity trajectory of generalized Couette flow by producing related flows, modifying boundary layer dynamics, or influencing flow equilibrium. In conclusion, the actual effect of a magnetic field being created on fluid speed in simple and generalized Couette flow is complicated and relies on a number of elements, comprising MHD implications, magnetic field force and direction, and equilibrium flow features. Furthermore, like (D_a) and (Re), the impact of ($H_2O + CU + TiO_2$) hybrid nanofluid is bit more than
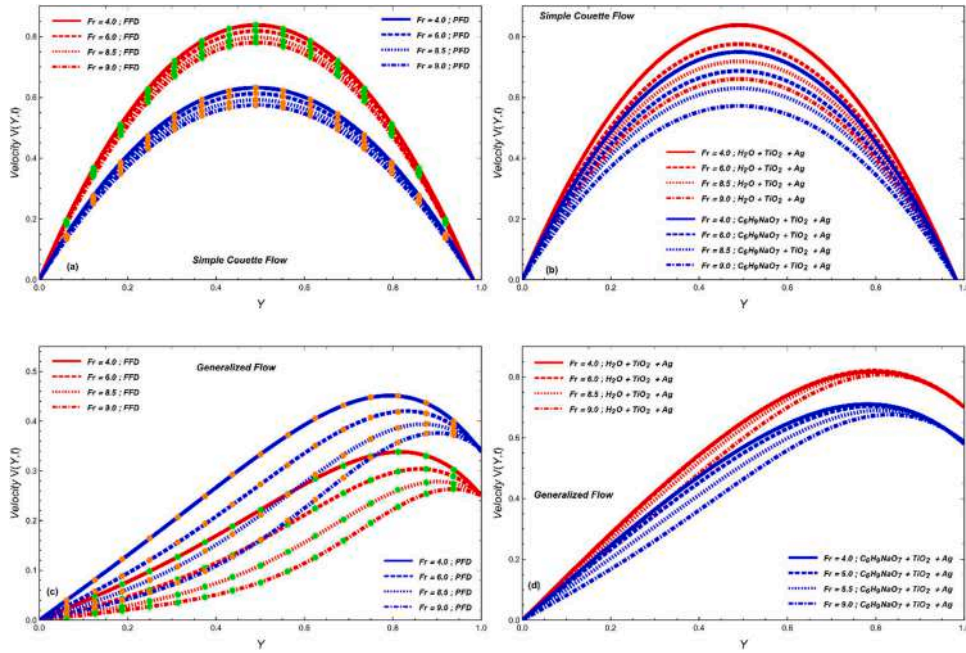
Fig. 11. Influence of *Fr* on $\wp(Y, \ell)$ with $\alpha = \beta = \gamma = 0.7$, $Re = 0.6$, $\mathscr{g} = \frac{\pi}{4}$, $M = 2.4$, $\Lambda_1 = 1.5$, $\ell = 1.4$, $D_a = 0.3$, $\varphi = 0.04$.

$(C_6H_9NaO_7 + CU + TiO_2)$ hybrid nanofluid for both parameters (M) and $(\mathscr{g})$ and for both simple and generalized flow cases.

Fig. 11(a-d) show the effect of Froude number (Fr) on the acceleration of $(H_2O + Ag + TiO_2)$ and $(C_6H_9NaO_7 + Ag + TiO_2)$-based hybrid nanofluid when using basic and generalized Couette flow. The Froude number (Fr) is a non-dimensional measure in fluids that describes the relative significance of inertial acceleration against gravity forces in a fluid's motion. In generalized Couette flow, when a fluid is trapped among two identical plates with relative movement, the Froude number might flow velocity since gravitational influences are often minimal in this setup. The Reynolds number (Re) represents the proportion of inertial and viscosity forces, which influences the stability of flow and conversion to disturbance. While the Froude number (Fr) might not

directly influence flow velocity in generalized Couette flow, it can nevertheless give insight into flow properties when combined with other dimensionless quantities. In addition, this can also be noted that the momentum profile attained by Fractal fractional derivative have more significant role as compared to Prabhakar solution velocity in the case of simple Couette flow. While on the other side, in the case of generalized flow, the behavior is altered due to the possessions of Mittag-Leffler kernel.

Fig. 12 (a-d) show the concrete actions of the Jeffery fluid restrictions (Λ_1) on the flow velocity for both basic and generalized Couette flows. The Jeffery fluid parameter (Λ_1) indicates the fluid's rate of relaxation divided by the flow's distinctive time range. It describes the fluid's elasticity and impacts its response to shear compression. As the
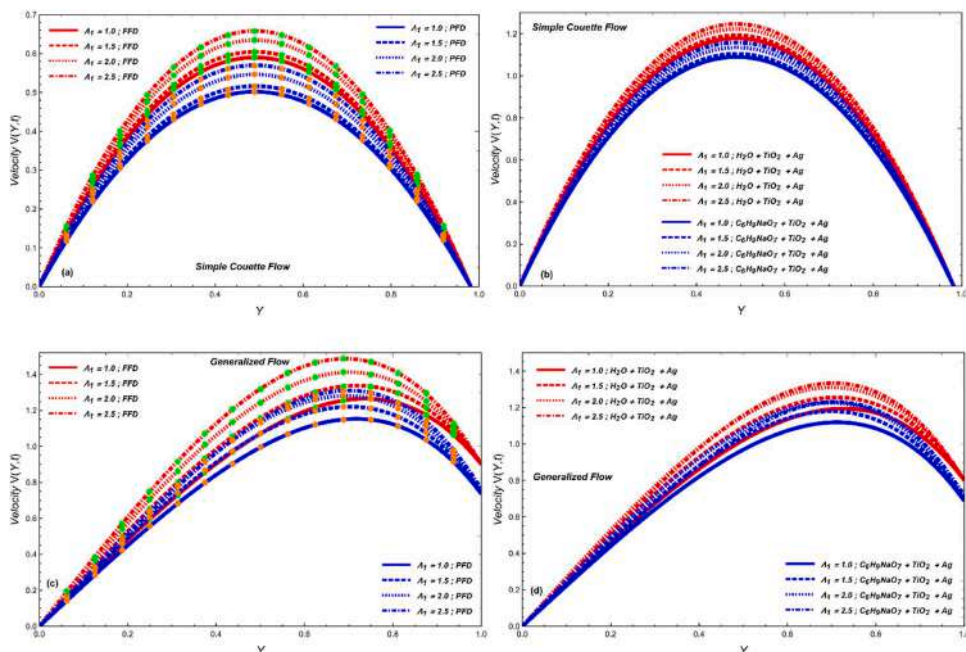
Fig. 12. Influence of Λ_1 on $\wp(Y, \ell)$ with $\alpha = \beta = \gamma = 0.7$, $Re = 0.6$, $\mathscr{g} = \frac{\pi}{4}$, $M = 2.4$, $Fr = 5.2$, $\ell = 1.4$, $D_a = 0.3$, $\varphi = 0.04$.
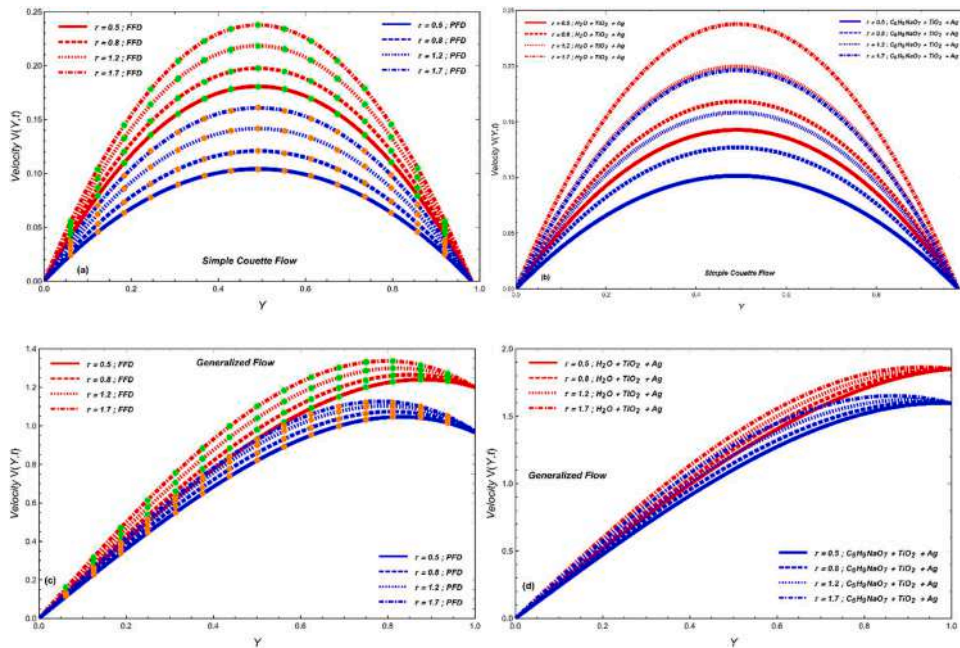
Fig. 13. Influence of t on $v(Y,t)$ with $\alpha = \beta = \gamma = 0.7$, $Re = 0.6$, $g = \frac{\pi}{4}$, $M = 2.4$, $Fr = 5.2$, $\Lambda_1 = 1.5$, $D_a = 0.3$, $\varphi = 0.04$.

Jeffery fluid component (Λ_1) grows, the viscoelastic implications grow more apparent. This indicates that the fluid is more deformation-resistant and may display stress relaxation or elastic rebound characteristics. Viscoelastic influences in Jeffery fluids can cause changes in the velocity distribution compared to Newtonian fluids. The Jeffery fluid characteristic may impact the variation in velocity and the entire form of the velocity profile as well. Increasing the value of the Jeffery fluid component (Λ_1) can lead to the development of thicker or more pronounced boundary layers, which in turn influence the velocity difference near the boundary layer and the overall flow dynamics. Consequently, as the value of (Λ_1) is increased, the flow profile exhibits a decrease.

Fig. 13 (a-d) show how time deletion (t) interacts with the acceleration field for both hybrid nanofluids ($C_6H_9NaO_7 + Ag + TiO_2$) and ($H_2O + Ag + TiO_2$). This shows that for simple and generalized Couette flow, the momentum field increases for both cases ($C_6H_9NaO_7 + Ag + TiO_2$) and ($H_2O + Ag + TiO_2$)-based hybrid nanofluids. Fluid speed can vary over time under temporary flow conditions. When a flow starts or stops or the boundary conditions change rapidly, the fluid motion does not immediately stabilize. On the other hand, the flow goes through

transitional phases in which the velocity changes over time until it stabilizes. Varying boundary conditions, such as the flow rate of a wall that interfaces with the fluid or the pressure gradient throughout a network, can reduce fluid velocity over time, as illustrated in Fig 12b. Furthermore, as with other limitations, the impact of ($H_2O + Ag + TiO_2$)-based suspension is somewhat greater than that of ($C_6H_9NaO_7 + Ag + TiO_2$)-based suspension with time value variations for both cases of velocity flows. Tables 1 and 2

Finally, Tables 3 and 4 compare the numerical findings of our investigation to the results obtained by Ramesh et al. [17] for both basic

Table 2
Basic characteristics of considered nanoparticles and base fluid.

Material	(H_2O)	$(C_6H_9NaO_7)$	(Ag)	(TiO_2)
$\rho(Kg/m^3)$	997.1	898	10,500	425
$C_p(J/kgK)$	4179	4175	235	6862
$k(W/mK)$	0.613	0.6367	429	8.9538
$\beta_T(K^{-1})$	21	23	1.89	0.9
σ	0.05	0.07	3.6×10^7	1×10^{-7}

Table 1
The thermo physical properties of basic quantities.

Thermal features	Hybrid Nanofluid
Density	$\rho_f = \dfrac{\rho_{hnf}}{\left((1-\varphi_2)\left((1-\varphi_1)+\varphi_1\frac{\rho_{s1}}{\rho_f}\right)+\varphi_2\rho_{s2}\right)}$
Dynamic Viscosity	$\mu_f = \mu_{hnf}(1-\varphi_1)^{2.5}(1-\varphi_2)^{2.5}$
Electrical conductivity	$\sigma_{bf} = \dfrac{\sigma_{hnf}}{\left(1+\frac{3\varphi(\varphi_1\sigma_1+\varphi_2\sigma_2-\sigma_{bf}(\varphi_1+\varphi_2))}{(\varphi_1\sigma_1+\varphi_2\sigma_2+2\varphi\sigma_{bf}-\varphi\sigma_{bf}(\varphi_1\sigma_1+\varphi_2\sigma_2-\sigma_{bf}(\varphi_1+\varphi_2)))}\right)}$
Thermal conductivity	$k_{bf} = \dfrac{k_{hnf}}{\left(\frac{k_{s2}+(n-1)k_{bf}-(n-1)(k_{bf}-k_{s2})\varphi_2}{k_{s2}+(n-1)k_{bf}+(k_{bf}-k_{s2})\varphi_2}\right)}$ and $k_f = \dfrac{k_{bf}}{\left(\frac{k_{s1}+(n-1)k_f-(n-1)(k_f-k_{s1})\varphi_1}{k_{s1}+(n-1)k_f+(k_f-k_{s1})\varphi_1}\right)}$
Heat capacitance	$(\rho C_p)_s = \dfrac{(\rho C_p)_{hnf}}{(1-\varphi_2)\left((1-\varphi_1)+\varphi_1\frac{(\rho C_p)_{s1}}{(\rho C_p)_f}\right)+\varphi_2(\rho C_p)_{s2}}$
Thermal Expansion Coefficient	$(\rho\beta)_f = \dfrac{(\rho\beta)_{hnf}}{(1-\varphi_2)\left((1-\varphi_1)+\varphi_1\frac{(\rho\beta)_{s1}}{(\rho\beta)_{f1}}\right)+\varphi_2(\rho\beta)_{s2}}$

Table 3
Comparison of *Couetteflow* with the results of Ramesh et al. [17].

y	$U(y, t)$ by this study for Couette flow	$U(y, t)$ by Ramesh et al. [17] for Couette flow
0.1	0.7717	0.8145
0.15	1.1393	1.2024
0.5	1.4853	1.5672
0.25	1.8029	1.9016
0.3	2.0854	2.1987
0.35	2.3269	2.4521
0.4	2.5216	2.6557
0.45	2.6643	2.8043
0.5	2.7507	2.8930
0.55	2.7765	2.9180
0.6	2.7391	2.8759
0.65	2.6354	2.7642
0.7	2.4639	2.5816
0.75	2.2235	2.3267
0.8	1.9138	2.0000
0.85	1.5354	1.6021
0.9	1.0891	1.1347

Table 4
Comparison of *generalizedcouetteflow* with the results of Ramesh et al. [17].

y	$U(y, t)$ by this study of generalized Couette flow	$U(y, t)$ by Ramesh et al. [17] for generalized Couette flow
0.1	0.4176	0.4251
0.15	0.6260	0.6373
0.5	0.8340	0.8492
0.25	1.0415	1.0605
0.3	1.2482	1.2712
0.35	1.4541	1.4812
0.4	1.6590	1.6904
0.45	1.8628	1.8986
0.5	2.0655	2.1057
0.55	2.2668	2.3118
0.6	2.4667	2.5166
0.65	2.6651	2.7202
0.7	2.8619	2.9224
0.75	3.0569	3.1223
0.8	3.2501	3.3224
0.85	3.4412	3.5198
0.9	3.6299	3.7153

and generalized Couette flows. The findings of this study for both scenarios (basic and generalized Couette flow) are extremely similar to those of Ramesh et al. [17], indicating its validity. Additionally, the velocity profile in both situations represents a diminishing trend.

5. Conclusions

The study investigated the implications of coupled heat and mass transfer on the rapid movement of a couple stress fluid through a porous medium, in the presence of a magnetized gradient within an inclined asymmetrical channel. The governing equations were formulated under the assumptions of long wavelengths and low Reynolds numbers. The study examined a fractional Jeffery-type hybrid nanofluid in the context of planar and generalized Couette flow phenomena. The fractional solutions for the stream function and thermal transport coefficients were derived using both the fractal and Prabhakar definitions of fractional derivatives. The second-degree PDE is examined using a numerical integral Laplace transformation. The impact of the included factors on the flow attributes and flow occurrences caused by wall digestion are thoroughly reviewed. The key conclusions of the examination are as follows:

- Increased coupling stress fluid factor leads to decreased peristaltic pumping speed.

In-plane and generalized Couette flows, the pressure progressive causes velocity to rise.

- Velocity rises as the time component improves.
- Increasing the heat production dimension, magnetic field tendency, and Jeffrey-fluid component leads to a drop in momentum.
- To interpret the Newtonian fluid system findings, set $\Lambda = 0$.
- The upward channel has a higher velocity than the horizontal stream.
- The velocity field may be altered by adjusting Re, Fr, M, Λ_1.
- The impression of (H_2O)-based hybrid nanofluid is a bit more than $(C_6H_9NaO_7)$-based hybrid nanofluid due to the corporeal features of considered nanoparticles (Ag, TiO_2).
- The Prabhakar fractional derivative-based models can also give a fascinating insight into the motion and other domain submissions, with the possibility to alter the boundary layers by adjusting fractional factors.
- The overlapping of this study's results with the consequences of Ramesh et al. [17] signifies the validity and correctness of the results of this study.
- The exposed solutions can aid in precisely interpreting actual data and serve as a tool for evaluating potential estimates of answers when required.

CRediT authorship contribution statement

Ali Raza: Writing – original draft, Methodology, Data curation, Conceptualization. **Ovidiu V. Stadoleanu:** Resources, Investigation, Formal analysis. **Ahmed M. Abed:** Writing – review & editing, Supervision, Data curation, Conceptualization. **Ali Hasan Ali:** Writing – review & editing, Visualization, Software, Project administration. **Mohammed Sallah:** Writing – original draft, Resources, Investigation, Funding acquisition.

Declaration of competing interest

The authors declare that they have no known competing financial interests or personal relationships that could have appeared to influence the work reported in this paper.

Data availability

No data was used for the research described in the article.

References

[1] S.U. Choi, "Nanofluids: from vision to reality through research," 2009.

[2] M. Turkyilmazoglu, Fully developed slip flow in a concentric annuli via single and dual phase nanofluids models, Comput. Methods Programs Biomed. 179 (2019) 104997.

[3] M. Sohail, R. Naz, S.I. Abdelsalam, On the onset of entropy generation for a nanofluid with thermal radiation and gyrotactic microorganisms through 3D flows, Phys. Scr. 95 (2020) 045206.

[4] I. Wole-Osho, E.C. Okonkwo, H. Adun, D. Kavaz, S. Abbasoglu, An intelligent approach to predicting the effect of nanoparticle mixture ratio, concentration and temperature on thermal conductivity of hybrid nanofluids, J. Therm. Anal. Calorim. 144 (2021) 671–688.

[5] I. Waini, A. Ishak, T. Groşan, I. Pop, Mixed convection of a hybrid nanofluid flow along a vertical surface embedded in a porous medium, Int. Commun. Heat Mass Transf. 114 (2020) 104565.

[6] N.S. Pandya, A.N. Desai, A.K. Tiwari, Z. Said, Influence of the geometrical parameters and particle concentration levels of hybrid nanofluid on the thermal performance of axial grooved heat pipe, Thermal Sci. Eng. Progress 21 (2021) 100762.

[7] A. Asadi, I.M. Alarifi, L.K. Foong, An experimental study on characterization, stability and dynamic viscosity of CuO-TiO2/water hybrid nanofluid, J. Mol. Liq. 307 (2020) 112987.

[8] S. Nadeem, N. Abbas, M. Malik, Inspection of hybrid based nanofluid flow over a curved surface, Comput. Methods Programs Biomed. 189 (2020) 105193.

[9] A.H. Al-Waeli, K. Sopian, M.T. Chaichan, H.A. Kazem, H.A. Hasan, A.N. Al-Shamani, An experimental investigation of SiC nanofluid as a base-fluid for a photovoltaic thermal PV/T system, Energy Convers. Manage 142 (2017) 547–558.

[10] N.A. Shah, A.A. Zafar, S. Akhtar, General solution for MHD-free convection flow over a vertical plate with ramped wall temperature and chemical reaction, Arab. J. Math. 7 (2018) 49–60.

[11] M. Caputo, M. Fabrizio, A new definition of fractional derivative without singular kernel, Progress Fractional Differ. Appl. 1 (2015) 73–85.

[12] A. Atangana and D. Baleanu, "New fractional derivatives with nonlocal and non-singular kernel: theory and application to heat transfer model," *arXiv preprint arXiv:1602.03408,* 2016.

[13] M. Yavuz, European option pricing models described by fractional operators with classical and generalized Mittag-Leffler kernels, Numer. Methods Partial. Differ. Equ 38 (2022) 434–456.

[14] A. Atangana, M.A. Khan, Validity of fractal derivative to capturing chaotic attractors, Chaos Solitons Fractals 126 (2019) 50–59.

[15] L. Kolsi, A. Raza, K. Al-Khaled, K. Ghachem, S.U. Khan, A.U. Haq, Thermal applications of copper oxide, silver, and titanium dioxide nanoparticles via fractional derivative approach, Waves Random Complex Media 33 (2023) 794–807.

[16] A. Raza, S.U. Khan, M.I. Khan, S. Farid, T. Muhammad, M.I. Khan, et al., Fractional order simulations for the thermal determination of graphene oxide (GO) and molybdenum disulphide (MoS2) nanoparticles with slip effects, Case Stud. Thermal Eng. 28 (2021) 101453.

[17] K. Ramesh, V. Joshi, Numerical solutions for unsteady flows of a magnetohydrodynamic Jeffrey fluid between parallel plates through a porous medium, Int. J. Comput. Methods Eng. Sci. Mech. 20 (2019) 1–13.

[18] Q. Haidong, M. ur Rahman, S.E. Al Hazmi, M.F. Yassen, S. Salahshour, M. Salimi, et al., Analysis of non-equilibrium 4D dynamical system with fractal fractional Mittag–Leffler kernel, Eng. Sci. Technol. Int. J. 37 (2023) 101319.

[19] F. Batool, A. Raza, S.U. Khan, M. Rafiq, M.I. Khan, Exploration of kink-type solutions of a dispersionless system using reliable techniques, Eur. Phys. J. Plus 138 (2023) 1074.

[20] A. Raza, S.U. Khan, M. Yasir, S. Dero, Accelerating flow for engine oil base fluid with graphene oxide and molybdenum disulfide nanoparticles: modified fractional simulations, Waves Random Complex Media (2023) 1–16.

[21] A. Raza, R. Ali, S.M. Eldin, S.H. Alfalqui, A.H. Ali, New fractional approach for CMC and water based hybrid nanofluid with slip boundary layer: applications of fractal fractional derivative, Case Stud. Thermal Eng. 49 (2023) 103280.

[22] S.U. Khan, A. Raza, A. Kanwal, The inclined surface flow of hybrid nanofluid with Newtonian heating and general velocity flow constraints: the Prabhakar model, Waves Random Complex Media (2022) 1–12.

[23] A.J. Chamkha, T. Groşan, I. Pop, Fully developed free convection of a micropolar fluid in a vertical channel, Int. Commun. Heat Mass Transf. 29 (2002) 1119–1127.

[24] J.C. Umavathi, A.J. Chamkha, A. Mateen, A. Al-Mudhaf, Unsteady two-fluid flow and heat transfer in a horizontal channel, Heat Mass Transf. 42 (2005) 81–90.

[25] S. Parvin, R. Nasrin, M. Alim, N. Hossain, A.J. Chamkha, Thermal conductivity variation on natural convection flow of water–alumina nanofluid in an annulus, Int. J. Heat. Mass Transf. 55 (2012) 5268–5274.

[26] A.J. Chamkha, Unsteady laminar hydromagnetic fluid–particle flow and heat transfer in channels and circular pipes, Int. J. Heat. Fluid. Flow. 21 (2000) 740–746.

[27] A. Raza, A.U. Haq, S. Farid, A Prabhakar fractional approach with generalized fourier law for thermal activity of non-newtonian second-grade type fluid flow: a fractional approach, Waves Random Complex Media (2022) 1–17.

[28] A. Raza, H.A. Hejazi, M.I. Khan, Impact of generalized fourier law in thermal flux convective flow over a vertical plate: analysis of fractional derivative, Int. J. Modern Phys. B 36 (2022) 2250162.

[29] N.A. Shah, C. Fetecau, D. Vieru, Natural convection flows of Prabhakar-like fractional Maxwell fluids with generalized thermal transport, J. Therm. Anal. Calorim. 143 (2021) 2245–2258.

[30] M.I. Asjad, A. Riaz, A.S. Alnahdi, S.M. Eldin, New solutions of fractional Jeffrey fluid with ternary nanoparticles approach, Micromachines (Basel) 13 (2022) 1963.

[31] N. Sarwar, M.I. Asjad, T. Sitthiwirattham, N. Patanarapeelert, T. Muhammad, A Prabhakar fractional approach for the convection flow of Casson fluid across an oscillating surface based on the generalized Fourier law, Symmetry (Basel) 13 (2021) 2039.

[32] C. Chen, A.U. Rehman, M.B. Riaz, F. Jarad, X.E. Sun, Impact of Newtonian heating via Fourier and Fick's laws on thermal transport of Oldroyd-B fluid by using generalized Mittag-Leffler kernel, Symmetry (Basel) 14 (2022) 766.

[33] A. Basit, M.I. Asjad, A. Akgül, Convective flow of a fractional second grade fluid containing different nanoparticles with Prabhakar fractional derivative subject to non-uniform velocity at the boundary, Math. Methods Appl. Sci. 46 (2023) 8148–8159.

[34] M. Samraiz, Z. Perveen, G. Rahman, K.S. Nisar, D. Kumar, On the (k,s)-Hilfer-Prabhakar fractional derivative with applications to mathematical physics, Front. Phys. 8 (2020) 309.

[35] T. Elnaqeeb, N.A. Shah, A. Rauf, Natural convection flows of carbon nanotube Prabhakar-like fractional second-grade nanofluids over an infinite plate with Newtonian heating, Math. Methods Appl. Sci. (2020).

[36] M. Aiyashi, S. Abo-Dahab, M.D. Albalwi, Effect of viscous dissipation and induced magnetic field on an unsteady mixed convective stagnation point flow of a nonhomogenous nanofluid, Sci. Rep. 13 (2023) 22529.

[37] K. Sudarmozhi, D. Iranian, I. Khan, A.S. Al-johani, S.M. Eldin, Magneto radiative and heat convective flow boundary layer in Maxwell fluid across a porous inclined vertical plate, Sci. Rep. 13 (2023) 6253.

[38] B. Kumar, G. Seth, R. Nandkeolyar, A. Chamkha, Outlining the impact of induced magnetic field and thermal radiation on magneto-convection flow of dissipative fluid, Int. J. Thermal Sci. 146 (2019) 106101.

[39] M.V. Krishna, A.J. Chamkha, Hall and ion slip effects on unsteady MHD convective rotating flow of nanofluids—application in biomedical engineering, J. Egyptian Math. Soc. 28 (2020) 1.

[40] X.J. Yang, Advanced Local Fractional Calculus and Its Applications, World Science Publisher, New York USA, 2012.

[41] J. Fan, J. He, Fractal derivative model for air permeability in hierarchic porous media, Abstract Appl. Anal. (2012).

[42] H.M. Srivastava, M. Izadi, Generalized shifted airfoil polynomials of the second kind to solve a class of singular electrohydrodynamic fluid model of fractional order, Fractal Fractional 7 (2023) 94.

[43] M. Imran, Application of fractal fractional derivative of power law kernel (FFP0Dxα, β) to MHD viscous fluid flow between two plates, Chaos Solitons Fractals 134 (2020) 109691.

[44] M. Aslam, M. Farman, H. Ahmad, T.N. Gia, A. Ahmad, S. Askar, Fractal fractional derivative on chemistry kinetics hires problem, AIMS. Math. 7 (2022) 1155–1184.

[45] O.T. Bafakeeh, A. Raza, S.U. Khan, M.I. Khan, A. Nasr, N.B. Khedher, et al., Physical interpretation of nanofluid (copper oxide and silver) with slip and mixed convection effects: applications of fractional derivatives, Appl. Sci. 12 (2022) 10860.

[46] Q. Ali, K. Al-Khaled, M.I. Khan, S.U. Khan, A. Raza, M. Oreijah, et al., Diffusion phenomenon for natural convection flow of classical Hartmann problem due to a cylindrical tube by generalized Fourier's theories: a Fractional analysis, Int. J. Modern Phys. B 37 (2023) 2350104.

[47] M.I. Khan, I.B. Mansir, A. Raza, S.U. Khan, S. Elattar, H.M. Said, et al., Fractional simulations for thermal flow of hybrid nanofluid with aluminum oxide and titanium oxide nanoparticles with water and blood base fluids, Nanotechnol. Rev. 11 (2022) 2757–2767.

[48] F. Afshari, S. Rahimpour, B. Sahin, B. Muratçobanoğlu, R. Teimuri-Mofrad, A review study on factors affecting the stability of nanofluids, Heat. Transf. Res. 53 (2022).

[49] F. Afshari, E. Mandev, S. Rahimpour, B. Muratçobanoğlu, B. Şahin, E. Manay, et al., Experimental and numerical study on air-to-nanofluid thermoelectric cooling system using novel surface-modified Fe3O4 nanoparticles, Microfluid Nanofluidics 27 (2023) 26.

[50] A. Raza, A. Ghaffari, S.U. Khan, A.U. Haq, M.I. Khan, M.R. Khan, Non-singular fractional computations for the radiative heat and mass transfer phenomenon subject to mixed convection and slip boundary effects, Chaos Solitons Fractals 155 (2022) 111708.

[51] M. Ghannam, M.Y. Selim, Viscoelastic performance evaluation of petrol oil and different macromolecule materials, Int. J. Thermofluids (2024) 100596.

[52] B.S. Abdullaeva, D. Abduvalieva, F.A. Rakhmatova, M.E. Yulchiev, Mathematical model of the solar combined cycle power plant using phase change materials in thermal energy storage system (Thermodynamic analysis), Int. J. Thermofluids 22 (2024) 100579.

[53] H.B. Bacha, N. Ullah, A. Hamid, N.A. Shah, A comprehensive review on nanofluids: synthesis, cutting-edge applications, and future prospects, Int. J. Thermofluids (2024) 100595.

[54] S. Alao, S. Salawu, R. Oderinu, A. Oyewumi, E. Akinola, Investigation of thermal radiation and viscous heating effects on the hydromagnetic reacting micropolar fluid species flowing past a stretchy plate in permeable media, Int. J. Thermofluids (2024) 100600.

[55] S. Azizifar, S. Mengjie, C.Y.H. CHAO, S.H. Hosseini, L. Pekař, A numerical study of multiphase flow boiling heat transfer of nanofluids in the horizontal metal foam tubes, Int. J. Thermofluids (2024) 100605.

[56] S.H.H. Karouei, M.B. Shani, S.H.H. Eimeni, P. Pasha, D.D. Ganji, Computational modeling of magnetized hybrid nanofluid flow and heat transfer between parallel surfaces with suction/injection, Int. J. Thermofluids 22 (2024) 100613.

[57] K. Trinh, Modelling the probability density distribution of the velocity in the wall layer of turbulent flow, in: 7th World Congress of Chemical Engineering: Proceedings, 2005.

[58] C.D. Andereck, S. Liu, H.L. Swinney, Flow regimes in a circular Couette system with independently rotating cylinders, J. Fluid. Mech. 164 (1986) 155–183.

[59] N. Liu, B. Khomami, Polymer-induced drag enhancement in turbulent Taylor-Couette flows: direct numerical simulations and mechanistic insight, Phys. Rev. Lett. 111 (2013) 114501.

[60] B.K. Jha, C.A. Apere, Time-dependent MHD Couette flow in a porous annulus, Commun. Nonlinear Sci. Numer. Simul. 18 (2013) 1959–1969.

[61] D. Eskin, Applicability of a Taylor–Couette device to characterization of turbulent drag reduction in a pipeline, Chem. Eng. Sci. 116 (2014) 275–283.

[62] R. Selvi, R. Muthuraj, MHD oscillatory flow of a Jeffrey fluid in a vertical porous channel with viscous dissipation, Ain Shams Eng. J. 9 (2018) 2503–2516.

[63] S. Srinivas, R. Muthuraj, Peristaltic transport of a Jeffrey fluid under the effect of slip in an inclined asymmetric channel, Int. J. Appl. Mech. 2 (2010) 437–455.

[64] Q. Ali, M. Amir, A. Raza, U. Khan, S.M. Eldin, A.M. Alotaibi, et al., Thermal investigation into the Oldroyd-B hybrid nanofluid with the slip and Newtonian heating effect: Atangana–Baleanu fractional simulation, Front. Mater. 10 (2023) 1114665.

[65] A. Raza, N. Nigar, U. Khan, S. Elattar, S.M. Eldin, A.M. Abed, Comparative investigation of fractional bioconvection and magnetohydrodynamic flow induced by hybrid nanofluids through a channel, Front. Mater. 10 (2023) 1143612.

[66] M. Ijaz Khan, K. Al-Khaled, A. Raza, S.U. Khan, J. Omar, A.M. Galal, Mathematical and numerical model for the malaria transmission: Euler method scheme for a malarial model, Int. J. Modern Phys. B 37 (2023) 2350158.